Robust Thermal Management in PEM Electrolysis: A Two-Loop Control Strategy

Islam Zerrougui Zhongliang Li Daniel Hissel

Université Marie et Louis Pasteur Université Marie et Louis Pasteur

UTBM, CNRS, Institut FEMTO-ST, UTBM, CNRS, Institut FEMTO-ST, Institut Universitaire de France (IUF)

Belfort, France Belfort, France

UTBM, CNRS, Institut FEMTO-ST,

Belfort, France

Abstract—Proton Exchange Membrane (PEM) electrolysis is a highly effective method for generating green hydrogen from renewable energy sources. However, effective thermal control is essential for maintaining high efficiency and prolonging the stack lifespan, especially under variable power conditions. This paper develops a four-state thermal model of the entire PEM electrolysis system, including key Balance of Plant (BoP) components such as heat exchangers and separators, to capture the system's primary temperature dynamics. Building on this model, we propose a two-loop control architecture: a slower PID loop regulates the inlet temperature, while a faster sliding-mode loop maintains a target temperature difference between the inlet and outlet temperatures. We use Particle Swarm Optimization (PSO) to determine the controller parameters, enabling robust operation under changing load conditions. Simulation results demonstrate that the proposed approach not only stabilizes the overall temperature but also mitigates abrupt disturbances from renewable energy sources, thereby improving both the efficiency and durability of the PEM electrolyzer.

PEM electrolysis, thermal management, nonlinear control, sliding mode, particle swarm optimization

I. INTRODUCTION

Proton Exchange Membrane (PEM) water electrolysis is a promising method for producing green hydrogen from water using electricity. Unlike alkaline or solid oxide electrolyzers, PEM stacks can tolerate rapid load changes and operate at high current densities, making them especially suited for coupling with intermittent wind or solar power. Effective thermal management is critical in PEM electrolysis systems, as temperature strongly influences both efficiency and system longevity. To ensure safe and optimal performance, most PEM electrolyzers are designed to operate between 40-70°C. Within this range, higher temperatures can reduce the membrane's ohmic resistance and improve reaction kinetics, increasing efficiency. However, elevated temperatures also accelerate thermal degradation and increase hydrogen crossover, affecting the stack's durability [1], [2]. Consequently, precise temperature regulation is essential to maximize both hydrogen yield and electrolyzer longevity.

Various models have been proposed in the literature to investigate the thermal behavior of electrolyzers. Ulleberg introduced a foundational linear lumped model for alkaline electrolysis [3], which was later adopted in works such as [4]–[6] to capture changes in the electrolyzer outlet temperature.

Stack temperature is governed by three variables: water flow rate, inlet water temperature, and the electrical current [7]. Because the current is fixed by the renewable power sources, only the first two can be adjusted in real time. A pump modulates the flow rate, carrying heat away as the water circulates through the electrolyzer and its auxiliaries, while a heat exchanger sets the desired inlet temperature.

Huang et al. [8] built a thermal model for alkaline electrolysis that regulates post-stack temperature with a proportional-integral (PI) controller. Qi et al. [9] extended the scope to the entire balance-of-plant, proposing a linearized, threestate space model and showing that Model Predictive Control (MPC) outperforms a feed-forward PID scheme. Dang et al. [10] coupled the electrolyzer to a coolant circuit via a logmean-temperature-difference (LMTD) method and validated a PID controller experimentally. For PEM electrolysis, Keller et al. [11] combined an adaptive PID controller with feedforward action, achieving markedly better disturbance rejection under variable wind-power profiles than a conventional PID. Collectively, these studies advance our understanding of thermal control in electrolyzers. Despite these numerous prior contributions, most works restrict attention to maintaining a single outlet or stack-average temperature. In practice, however, the temperature rise across the stack (i.e., $T_{out} - T_{in}$) can reach several kelvins under heavy load, causing localized overheating of terminal cells. Excessive temperature difference not only accelerates membrane degradation in those hot cells but also increases mechanical stress and hydrogen crossover, compromising safety and durability. To the best of our knowledge, no existing controller simultaneously regulates both the absolute stack temperature and the inlet-outlet temperature differential.

In response to these gaps, this paper presents a comprehensive model that characterizes temperature dynamics across major components of a PEM electrolyzer. We formulate a four-state representation of the system's thermal behavior and develop a nonlinear control strategy to handle disturbances arising from renewable energy variability. This control scheme not only maintains the electrolyzer's temperature at its setpoint but also actively regulates the inlet-to-outlet temperature differential, enhancing overall thermal management. Finally, we employ a Particle Swarm Optimization (PSO) algorithm to tune the controller parameters,

ensuring robust performance across a wide range of operating conditions.

The remainder of this paper is organized as follows. In Section II, we introduce the PEM electrolyzer's principal components and derive their corresponding temperature models. Section III presents the design and methodology of the proposed control strategy. Section IV presents the control design. Finally, Section V showcases MATLAB/Simulink simulation results, demonstrating the robustness of our control approach.

II. TEMPERATURE MODEL OF THE PEM ELECTROLYSIS

In this section, we formulate a model that tracks temperature variations in each component of the PEM electrolysis system. We focus on the anode side, where water is supplied and consumed. On this side, the outlet temperature can rise significantly higher than on the cathode side due to the higher overvoltage [7]. Figure 1 illustrates the PEM electrolysis system's layout and highlights the key hardware required for safe, efficient operation: two pumps, a heat exchanger, a separator, and the PEM electrolyzer. The two pumps fulfill complementary tasks. The first circulates water through the electrolyzer loop (hot side), whereas the second delivers cooling water to the heat-exchanger loop (cold side). Precise control of both pumps is essential for effective temperature regulation.

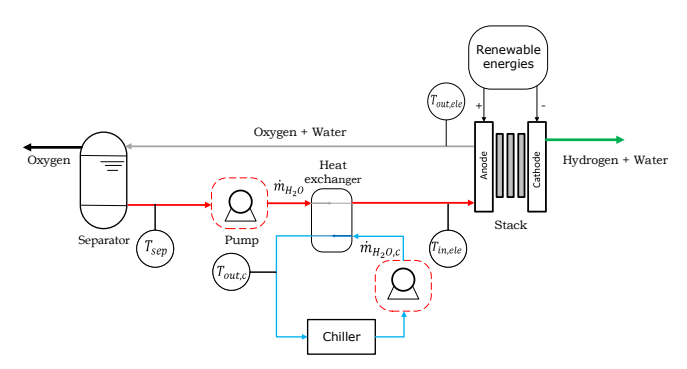


Fig. 1: Schematic of the temperature distribution in the PEM electrolysis system

The following subsections briefly describe each component shown in Fig. 1 and introduce corresponding models that capture their thermal behavior.

A. PEM electrolysis

As the PEM electrolyzer lies at the heart of our control objectives, its temperature dynamics demand careful attention. In this section, we treat the electrolyzer as a lumped-parameter model whose behavior is governed by water flow rate, inlet water temperature, and current density. Additionally, geometric characteristics such as the number of cells and the total active area significantly influence how its temperature evolves. To capture these thermal effects, we account for both the heat generated within the stack and the heat lost to the surroundings. The resulting temperature

model is summarized as follows:

$$C_{th}\dot{T}_{out,ele} = \dot{Q}_{gen} - \dot{Q}_{loss} - \dot{Q}_{cool} \tag{1}$$

 $T_{out,ele}$ is the outlet temperature of the electrolyzer, and C_{th} is the total thermal capacitance of the stack. The three terms on the right are defined as follows:

 \dot{Q}_{gen} is the heat produced by the electrochemical reactions, and can be expressed as follows:

$$\dot{Q}_{qen} = n_{cell} I (V_{cell} - V_{th}) \tag{2}$$

in which n_{cell} is the number of cells, I is the current applied, V_{cell} is the voltage applied on one cell, V_{th} is the thermodynamic voltage. The applied voltage can be empirically calculated as a function of current and temperature, as proposed by Ulleberg et al. [12], by the following expression:

$$V = V_{rev} + \frac{r_1 + r_2 T}{A} I + (s + s_1 T + s_2 T^2) \log\left(\frac{t_1 + t_2 T + t_3 T^2}{A} I + 1\right).$$
(3)

In which r_1 , r_2 , s, s_1 , s_2 , t_1 , t_2 , and t_3 are fitting parameters, and A is the surface area of the stack.

The term \dot{Q}_{loss} denotes the heat lost during electrolysis, mainly via convection and radiation [13]:

$$\dot{Q}_{loss} = \dot{Q}_{conv} = h A \left(T_{out,ele} - T_{amb} \right) \tag{4}$$

Here, and T_{amb} is the ambient temperature, h is an effective heat-transfer coefficient (convection + radiation).

Finally, \dot{Q}_{cool} represents the cooling loss that is caused by the feed water, this can be represented as follows:

$$\dot{Q}_{cool} = \dot{m}_{H_2O}c_{p,H_2O}(T_{out,ele} - T_{in,ele}) \tag{5}$$

 \dot{m}_{H_2O} is the water flow that goes through the electrolysis, c_{p,H_2O} is the specific heat capacity of water, $T_{in,ele}$ is the temperature inlet of the stack.

Eq. (1) captures the stack's net heat accumulation, generated heat from cell overpotentials, lumped heat-losses, and removal by coolant flow.

B. Heat exchanger

Heat exchange is a key part of the PEM electrolyzer's BoP. The heat exchanger maintains the desired operating temperature by heating or cooling the water as it flows through the system. The heat exchanger has two inlets and two outlets, forming two independent loops. The first loop (hot side) is connected to the PEM electrolyzer and its pump; the second loop (cold side) is driven by another pump and use to cool the water in the first loop (see Fig. 1). Inside the heat exchanger, the two loops exchange thermal energy. We model each side with a lumped thermal capacitance and a convective heat-transfer term as follows [13]:

$$C_{h}\dot{T}_{in,ele} = \dot{m}_{H_{2}O}c_{ph}(T_{sep} - T_{in,ele}) - UA_{ex}(T_{in,ele} - T_{out,c})$$

$$C_{c}\dot{T}_{out,c} = \dot{m}_{H_{2}Oc}c_{pc}(T_{in,c} - T_{out,c}) - UA_{ex}(T_{out,c} - T_{in,ele})$$
(6)

in which A_{ex} is the heat transfer area, U is the overall heat transfer coefficient, and \dot{m}_{H_2Oc} is the cold water flow.

While most of the research in the literature tends to linearize the heat exchanger model, in this work, we will treat it as a nonlinear system.

C. Separator

After the stack, a gas-liquid separator removes hydrogen/oxygen from the water and returns liquid to the hot loop. We model the separator as a lumped thermal mass at temperature T_{sep} . The separator sees inflow at $T_{out,ele}$ (stack outlet) and outflow to the pump at T_{sep} . We also account for heat loss from the separator vessel to the ambient. Thus the separator model can be represented as follows:

$$C_{sep} \frac{dT_{sep}}{dt} = \dot{m}_{H_2O} c_{p,H_2O} (T_{out,ele} - T_{sep}) - \frac{1}{R} (T_{sep} - T_{amb})$$
(7)

 C_{sep} is the heat capacitance of the separator, T_{sep} represent the temperature in the outlet of the separator, R represent the separator's thermal resistance.

In this study, we assume that the mass flows on the hot and cold sides are proportional to the control inputs y_h, y_c which represent two valves. Specifically:

$$\dot{m}_{H_2O} = y_h v_{H_2O} \tag{8}$$

$$\dot{m}_{H_2Oc} = y_c v_{H_2O} \tag{9}$$

where v_{H_2O} is the nominal pump flow rate. Given that the pump dynamics occur on a faster timescale than the thermal processes, we neglect their dynamics.

III. CONTROL-ORIENTED MODEL FOR PEM ELECTROLYSIS

A control-oriented model collects the physically derived heat-balance equations into a standard state-space form. This makes it easier to spot the primary nonlinearities and to design suitable control laws. In general, a nonlinear statespace model is written as:

$$\dot{x} = f(x, u, t). \tag{10}$$

From the modeling of the electrolysis chain (Section 2), it is clear that the system features four temperature states: $T_{out,ele}$, $T_{in,ele}$, $T_{out,c}$, T_{sep} ,

and two valve-controlled inputs governing water flow:

- u_1 : normalized valve positions of the main (hot) circuit.
- u₂: normalized valve positions of the cooling water flow

The control-oriented model is summarized by defining the states and inputs as:

$$\begin{pmatrix} x_1 \\ x_2 \\ x_3 \\ x_4 \end{pmatrix} = \begin{pmatrix} T_{out,ele} \\ T_{in,ele} \\ T_{out,c} \\ T_{sep} \end{pmatrix} \quad \text{and} \quad \begin{pmatrix} u_1 \\ u_2 \end{pmatrix} = \begin{pmatrix} y_h \\ y_c \end{pmatrix}.$$
 (11)

Rearranging the equations derived in Section 2 leads to the following nonlinear state-space form:

$$\dot{x} = \begin{pmatrix} \dot{x}_1 \\ \dot{x}_2 \\ \dot{x}_3 \\ \dot{x}_4 \end{pmatrix} = \begin{pmatrix} -C_2 x_1 + C_3 (x_1 - x_2) u_1 + D(i), \\ C_5 (x_3 - x_2) + C_4 (x_4 - x_2) u_1, \\ C_6 (x_2 - x_3) + C_7 (T_{in,c} - x_3) u_2, \\ -C_9 x_4 + C_{10} (x_1 - x_4) u_1 - C_{11}. \end{pmatrix},$$
(12)

The constants C_2, C_3, \dots, C_{11} represent lumped coefficients derived from system parameters, as given by

$$D(i) = \frac{n_{cell}I(V_{cell} - V_{th})}{C_{th}} + \frac{hAT_{amb}}{C_{th}}, \quad C_2 = \frac{hA}{C_{th}},$$

$$C_3 = \frac{v_{H_2O} c_{p,H_2O}}{C_{th}}, C_4 = \frac{v_{H_2O} c_{p,h}}{C_h}, C_5 = \frac{U A_{ex}}{C_h},$$

$$C_6 = \frac{U A_{ex}}{C_c}, C_7 = \frac{v_{H_2O} c_{p,c}}{C_c}, C_8 = \frac{v_{H_2O} c_{p,c} T_{in,c}}{C_c},$$

$$C_9 = \frac{h_s}{C_{sep}}, C_{10} = \frac{v_{H_2O} c_{p,H_2O}}{C_{sep}}, C_{11} = \frac{h_s T_{amb}}{C_{sep}}.$$

A. Bilinear State-Space Form

To highlight the structure of the model and to facilitate subsequent control design, the four temperature balances can be represented in matrix form, resulting in the bilinear statespace representation

$$\dot{\mathbf{x}} = \left(\bar{A} + u_1 N_1 + u_2 N_2\right) \mathbf{x} + B \mathbf{u} + \mathbf{d}. \tag{13}$$

In which

$$\bar{A} = \begin{bmatrix} -C_2 & 0 & 0 & 0 \\ 0 & -C_5 & C_5 & 0 \\ 0 & C_6 & -C_6 & 0 \\ 0 & 0 & 0 & C_9 \end{bmatrix} \quad N_1 = \begin{bmatrix} C_3 & -C_3 & 0 & 0 \\ 0 & -C_4 & 0 & C_4 \\ 0 & 0 & 0 & 0 \\ C_{10} & 0 & 0 & -C_{10} \end{bmatrix}$$

Here \bar{A} gathers the purely linear heat-transfer terms, N_1 and N_2 capture the bilinear couplings with the hot and cold inputs, B contains the direct (non-bilinear) input path. \mathbf{d} is a constant/disturbance vector (heat from overvoltage and ambient losses).

Comment on Nonlinearities

Because each valve input u_i multiplies temperature differences (e.g., $(x_1-x_2)u_1$ or $(T_{in,c}-x_3)u_2$), the system is bilinear. Moreover, D(i) in \dot{x}_1 acts as a time-varying disturbance arising from stack current and ambient conditions. These bilinear couplings and disturbances motivate the use of robust or sliding-mode control to maintain tight temperature regulation under variable operating conditions.

Overall, this bilinear model enables the design of control laws that adjust u_1 and u_2 to regulate both inlet and outlet temperatures, even in the presence of time-varying disturbances.

IV. CONTROL DESIGN

Because valve inputs u_1 and u_2 each affect both stack inlet and outlet temperatures, attempting to regulate $\{T_{in,ele},T_{out,ele}\}$ with two independent loops leads to 'loop-fighting': any adjustment to fix $T_{in,ele}$ disturbs $T_{out,ele}$, and vice versa. Instead, we adopt a robust two-loop control strategy to ensure both stable operation and fast disturbance rejection. This approach decouples the regulation problem into two distinct loops, one for the inlet temperature control and another for the outlet–inlet temperature difference control. We define new outputs

$$z_1 = T_{in.ele}, \quad z_2 = T_{out.ele} - T_{in.ele} = \Delta T.$$

In these coordinates, the system acquires a cascade-like (lower-triangular) form:

$$\dot{z}_1 = f_1(z_1, u_1, u_2), \quad \dot{z}_2 = f_2(z_1, z_2, u_1, u_2).$$

Now, Loop 1 needs only to regulate z_1 (stack inlet temperature) without knowing z_2 . Loop 2 regulates z_2 using z_1 as a known feedforward. This two-loop structure prevents control conflicts and enables each loop to be tuned independently.

Fig. 2 illustrates the schematic of the two-loop thermal control strategy. This approach is motivated by the need to address both slow and fast dynamics within the system:

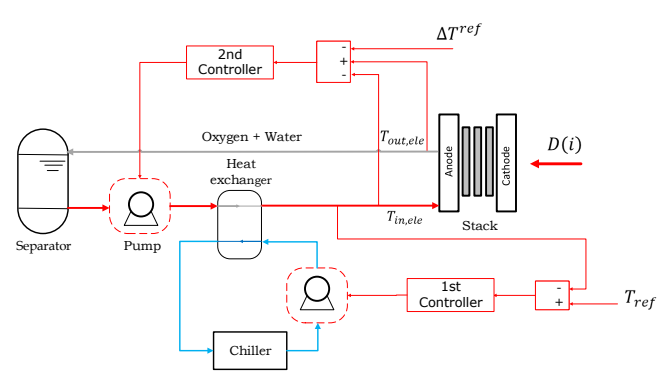


Fig. 2: Schematic of the two-loop thermal control strategy for the PEM electrolysis system

A. Loop 1: Inlet Temperature Control (Slower Loop)

The first control loop is responsible for regulating the inlet temperature $T_{in,ele}$ to its desired set point. This regulation is achieved by manipulating the flow rate through the first pump, which supplies water to the heat exchanger and chiller. Given that changes in $T_{in,ele}$ occur gradually, a conventional PID controller is employed. This controller is tuned to provide stable tracking and to prevent large drifts in the overall system temperature.

The PID control law is then given by

$$e_1(t) = T_{ref} - T_{in,ele}(t),$$

$$u_{PID}(t) = K_p e_1(t) + K_i \int_0^t e_1(\tau) d\tau + K_d \frac{d}{dt} e_1(t).$$

where K_p , K_i , and K_d are the proportional, integral, and derivative gains, respectively.

B. Loop 2: Temperature Difference Control (Faster Loop)

Once the inlet temperature is adequately controlled, the focus shifts to maintaining a precise temperature difference between the outlet and the inlet. The control objective for this loop is to ensure:

$$\Delta T = T_{out.ele} - T_{in.ele} = \Delta T^{ref}$$
,

where ΔT^{ref} is the desired temperature gradient. A robust sliding-mode controller is implemented to handle the fast dynamics and mitigate the impact of uncertainties. Specifically, the super-twisting algorithm STA is employed [14]. This approach enhances robustness by ensuring finite-time convergence and reducing the sensitivity to parameter variations and external disturbances. In addition, a first-order low-pass filter is integrated into the control loop to suppress chattering, improving the smoothness and reliability of the control action. In this case, the sliding surface is represented by the error and its derivative. Using a STA controller, the control input is given by

$$u(t) = -k_1 |s|^{1/2} \operatorname{sgn}(s) - k_2 \int_0^t \operatorname{sgn}(s) d\tau,$$

where $k_1 > 0$ and $k_2 > 0$ are the controller gains. To reduce chattering, a first-order low-pass filter is applied to u(t):

$$\tau_f \dot{u}_f(t) + u_f(t) = u(t),$$

so that the final control signal applied to the plant is $u_f(t)$. This control law ensures that the error s converges to zero in finite time, even in the presence of disturbances and uncertainties.

C. Controller Parameter Tuning

Achieving robust performance across both control loops necessitates precise tuning of the controller parameters. In this work, PSO is utilized. PSO is selected for its ease of implementation and effectiveness in navigating high-dimensional parameter spaces. By systematically exploring the parameter space, PSO converges on a set of controller parameters that balance tracking accuracy with control effort, ensuring that the system can handle varying operating conditions while maintaining robust thermal regulation.

V. SIMULATION AND RESULTS

In this section, we present simulation results that demonstrate the effectiveness of the proposed two-loop thermal control strategy. All simulations were performed in MAT-LAB/Simulink using the nonlinear, four-state thermal model of the PEM electrolysis system described in Section IV. A random current input, shown in Fig. 3, emulates fluctuations in a renewable power source to test the robustness of the control strategy under real-world conditions. The simulation is run for 4000 seconds, starting from an initial input stack temperature of 318 K.

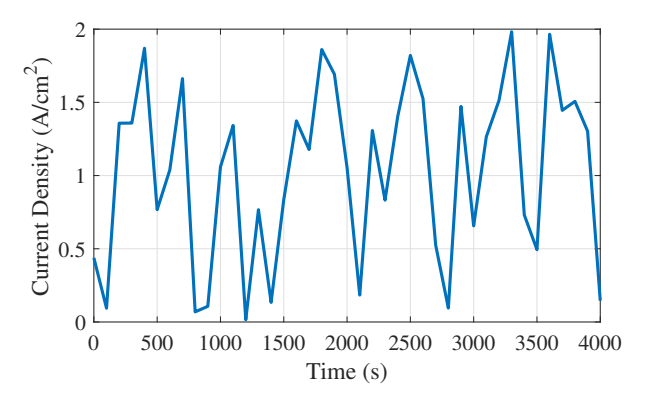


Fig. 3: Current input profile applied to the PEM electrolysis system

The primary control objective at this stage is to regulate the inlet temperature of the electrolysis process, a task managed primarily by the heat exchanger circuit. Fig. 4(a) illustrates how the inlet temperature (blue line) evolves over time in comparison to the reference (orange line). Initially, the reference is set to 315 K, and at t=2000 s, it increases to 320 K. The results indicate that the inlet temperature closely tracks the desired setpoint throughout the simulation, exhibiting minimal overshoot and a short settling time of about 8 min. Notably, the controller handles the step change at 2000 s smoothly, demonstrating strong disturbance rejection and

adaptability to changing thermal demands. These findings confirm that the outer-loop PID controller can maintain an accurate inlet temperature under varying conditions, thereby establishing a stable thermal foundation for the electrolysis system.

Fig. 4(c) illustrates the PID control signal that manipulates the cooling water flow to maintain the desired inlet temperature. Although small fluctuations appear (mostly caused by the hot controller u_1), these variations do not prevent the inlet temperature from converging to its setpoint, indicating effective coordination between the two loops. Moreover, the negligible steady-state error at both reference levels and the smooth transient response confirm that the PID loop is adequately tuned.

The control system's second objective is to maintain a specified temperature differential of 5 K between the electrolyzer's inlet and outlet. This target ensures a more uniform temperature distribution along the anode channel, since large gradients would indicate significantly higher reaction rates near the outlet compared to the inlet—potentially leading to uneven membrane utilization and accelerated wear at high current densities. To evaluate the effectiveness of the STA controller, its performance was compared against a well-tuned PID.

Figure 4(b) illustrate the temperature-difference tracking for both the STA and a conventional PID controller acting

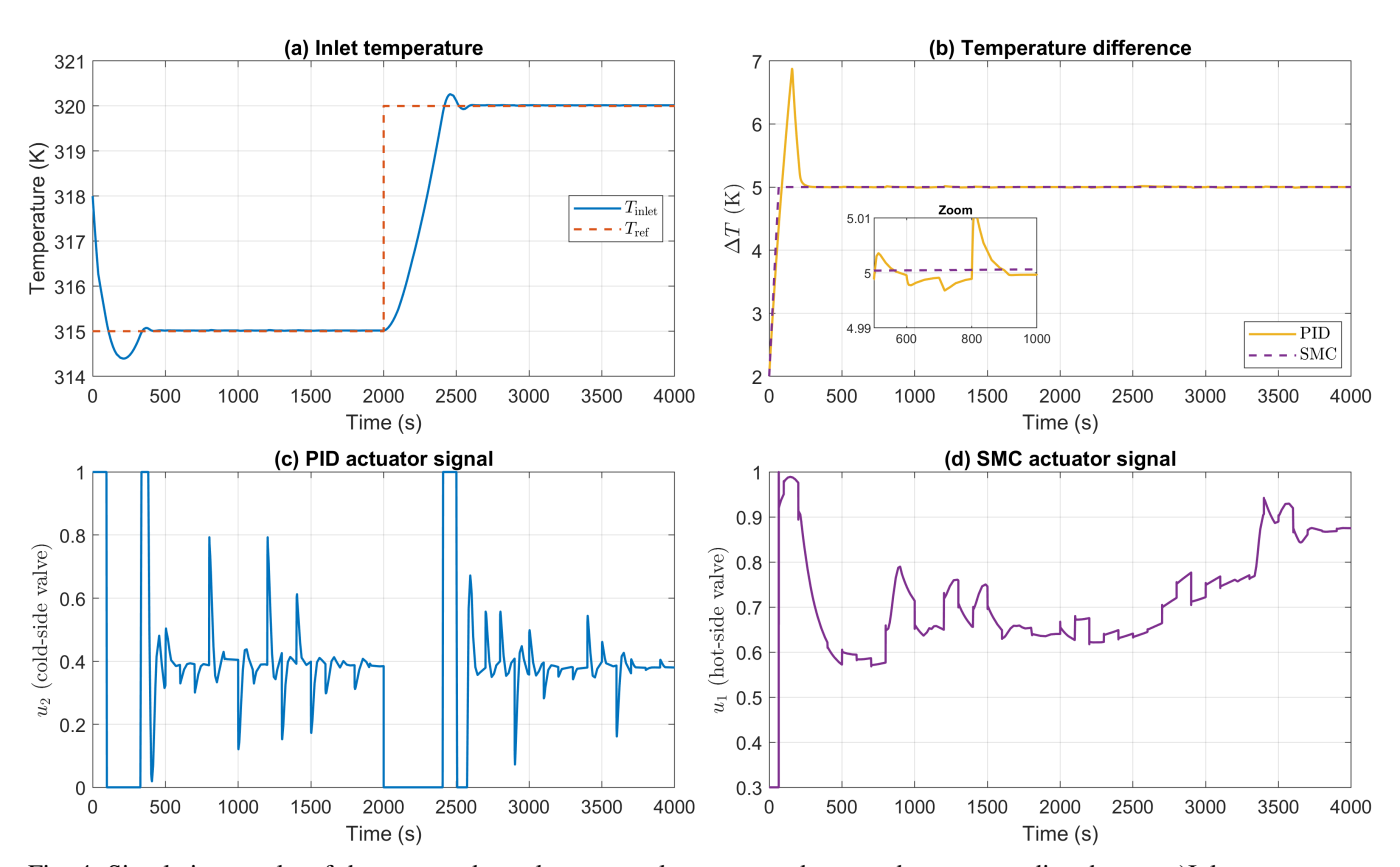


Fig. 4: Simulation results of the proposed two-loop control strategy under a random current disturbance: a)Inlet temperature tracking, , b)Temperature difference tracking, (c) PID control signal for the slower loop, and(d) Sliding-mode control signal for the faster loop.

directly on ΔT . Under the same random current profile, the PID loop exhibits a noticeable overshoot (peaking near 6.8 K) and slightly rings around the 5 K setpoint in response to the disturbance. By contrast, the STA controller drives ΔT to 5 K with almost no overshoot and negligible oscillation. In both cases, variations in the inlet temperature and current profile, disturb ΔT , however, the sliding-mode law rejects those disturbances in finite time and maintain robust performance. For mild or slowly varying load changes, the PID controller alone can already keep ΔT within acceptable bounds..

Fig. 4(d) shows the control input associated with the fast loop, which is responsible for temperature-difference control. Its profile reveals how the system adjusts cooling capacity in real-time to compensate for both the random load current and any inlet-temperature variations. The sliding-mode algorithm maintains a stable output, with minimal chattering due to the implemented first-order filtering. Overall, this confirms that the second loop robustly cancels disturbances introduced by shifts in the inlet temperature and load current, allowing the temperature difference to remain within tight bounds and ensure stable temperature distribution through the anode channel.

Overall, the simulations confirm that splitting thermal control into two loops, one for the slower inlet-temperature dynamics and one for the faster temperature-difference regulation, yields robust, stable performance. The PID loop handles gradual disturbances and set-point changes in the inlet temperature, while the super-twisting sliding-mode controller quickly compensates for fluctuations in stack heat generation to maintain a nearly constant temperature gradient. This decoupling ensures both the overall operating temperature and the local temperature distribution across the stack remain within desirable limits, which can improve electrolysis efficiency and extend stack life.

VI. CONCLUSION

This study presented a comprehensive bilinear model for PEM electrolysis, incorporating both the electrolyzer stack and critical BoP elements to accurately represent temperature variations throughout the system. Guided by this model, we implemented a two-loop control strategy that separately addresses slow and fast thermal dynamics. A PID controller was used to stabilize the inlet temperature, while a sliding-mode algorithm governed the outlet–inlet temperature difference. Through Particle Swarm Optimization (PSO), we efficiently determined the control gains, striking a balance between robust disturbance rejection and minimal control effort.

Simulation results under a random current profile showed that the PID loop successfully maintained a stable inlet temperature with minimal overshoot, while the sliding-mode controller drove the temperature difference to its setpoint with negligible oscillation—even in the presence of inlet-temperature disturbances. A direct comparison with a PID acting on the temperature difference demonstrated the superior disturbance-rejection and finite-time convergence of the

super-twisting law. Overall, the decoupled two-loop design preserves both global stack temperature and local thermal uniformity, thereby improving electrolysis efficiency and mitigating degradation in the end cells.

Moving forward, the proposed model and two-loop control strategy will be validated through experimental testing on a physical PEM electrolyzer setup. The experimental validation will further refine the control gains and pave the way for practical implementation in industrial-scale PEM electrolysis systems.

ACKNOWLEDGMENT

This work has been supported by the EIPHI Graduate School (contract ANR-17-EURE-0002) and the Region Bourgogne Franche-Comté.

REFERENCES

- Qi Feng, Gaoyang Liu, Bing Wei, Zhen Zhang, Hui Li, Haijiang Wang, et al. A review of proton exchange membrane water electrolysis on degradation mechanisms and mitigation strategies. *Journal of Power* Sources, 366:33–55, 2017.
- [2] Patrick Trinke, Boris Bensmann, Sven Reichstein, Richard Hanke-Rauschenbach, and Kai Sundmacher. Impact of pressure and temperature on hydrogen permeation in pem water electrolyzers operated at asymmetric pressure conditions. ECS Transactions, 75(14):1081, 2016
- [3] Øystein Ulleberg. Modeling of advanced alkaline electrolyzers: a system simulation approach. *International journal of hydrogen energy*, 28(1):21–33, 2003.
- [4] Islam Zerrougui, Zhongliang Li, and Daniel Hissel. Investigating bubble impacts on pem electrolysis performance through enhanced multiphysics modeling. *International Journal of Hydrogen Energy*, 98:626–638, 2025.
- [5] ME Lebbal and Stéphane Lecœuche. Identification and monitoring of a pem electrolyser based on dynamical modelling. *International* journal of hydrogen energy, 34(14):5992–5999, 2009.
- [6] Rafael García-Valverde, Nieves Espinosa, and Antonio Urbina. Simple pem water electrolyser model and experimental validation. *interna-tional journal of hydrogen energy*, 37(2):1927–1938, 2012.
- [7] Islam Zerrougui, Zhongliang Li, and Daniel Hissel. Physics-informed neural network for modeling and predicting temperature fluctuations in proton exchange membrane electrolysis. *Energy and AI*, page 100474, 2025.
- [8] Chunjun Huang, Xin Jin, Yi Zong, Shi You, Chresten Træholt, and Yi Zheng. Operational flexibility analysis of alkaline electrolyzers integrated with a temperature-stabilizing control. *Energy Reports*, 9:16–20, 2023.
- [9] Ruomei Qi, Jiarong Li, Jin Lin, Yonghua Song, Jiepeng Wang, Qiangqiang Cui, Yiwei Qiu, Ming Tang, and Jian Wang. Thermal modeling and controller design of an alkaline electrolysis system under dynamic operating conditions. *Applied Energy*, 332:120551, 2023.
- [10] Jian Dang, Fuyuan Yang, Yangyang Li, Yingpeng Zhao, Minggao Ouyang, and Song Hu. Experiments and microsimulation of highpressure single-cell pem electrolyzer. *Applied Energy*, 321:119351, 2022
- [11] R Keller, E Rauls, M Hehemann, M Müller, and M Carmo. An adaptive model-based feedforward temperature control of a 100 kw pem electrolyzer. *Control Engineering Practice*, 120:104992, 2022.
- [12] Øystein Ulleberg. Stand-alone power systems for the future: optimal design, operation and control of solar-hydrogen energy systems. 1998.
- [13] Frank P Incropera, David P DeWitt, Theodore L Bergman, Adrienne S Lavine, et al. Fundamentals of heat and mass transfer, volume 6. Wiley New York, 1996.
- [14] K David Young, Vadim I Utkin, and Umit Ozguner. A control engineer's guide to sliding mode control. *IEEE transactions on control* systems technology, 7(3):328–342, 1999.